IEEE Access
Multidisciplinary | Rapid Review | Open Access Journal

Received November 2, 2019, accepted November 19, 2019, date of publication November 27, 2019,
date of current version December 12, 2019.

Digital Object Identifier 10.1109/ACCESS.2019.2956256

A Novel Online Estimation and Compensation Method for Strapdown Phased Array Seeker Disturbance Rejection Effect Using Extended State Kalman Filter

SHIH-YAO LIN, DEFU LIN, AND WEI WANG
School of Aerospace Engineering, Beijing Institute of Technology, Beijing 100081, China
Corresponding author: Shih-Yao Lin (3120185050@bit.edu.cn)

This work was supported by the Natural Science Foundation of China under Grant 61903350.

ABSTRACT The radome error and beam pointing error found commonly in the strapdown phased array radar seeker can cause coupling between the missile body motion and the seeker model, impacting the output precision of the seeker and causing the disturbance rejection effect (DRE). Aiming to address the serious impact of DRE on the missile guidance and control system, a strapdown phased array radar seeker DRE parasitic loop (considering radome error and beam pointing error) is established. The DRE parasitic loop is analyzed. The main aim of this paper was to develop a novel online estimation and compensation method for a DRE parasitic loop using an extended state Kalman filter, which was compared with an extended Kalman filter and a strong tracking unscented Kalman filter. The simulation results show that the proposed online estimation and compensation method for the DRE parasitic loop can estimate the radome error slope and beam pointing error slope stably and accurately from the initial velocity pointing error input and the large initial estimation error. Effective suppression of the DRE problem and compensation for the line-of-sight angular rate output in real time is achieved. Furthermore, the guidance system performance and precision are both improved.

INDEX TERMS Active disturbance rejection control, beam pointing error, disturbance rejection effect parasitic loop, extended state Kalman filter, radome error.

I. INTRODUCTION

Certain missiles with strapdown phased array radar seekers have radomes, which are structures attached to the noses of the missiles. The function of the radome is to transmit the incoming radar wave without loss or distortion and to withstand the structural and thermal loads induced by supersonic travel. The refraction of the electromagnetic wave by the radome causes an error in the line-of-sight (LOS) angle known as the radome refraction angle [1]. Although this refraction angle is small (generally less than one degree), its angular rate of change can cause guidance problems because it creates a parasitic loop within the guidance homing loop. The consequence of the destabilizing effect is an increase in miss distance. Unlike traditional gimbal mechanical scanning seekers, the phased array radar seeker is usually strapped on the missile body and conducts beam scanning via the phase shift value of the element's radiation from the phase shifter. Hence, the performance of the digital phase shifter determines the performance of the seeker beam scanning. Considering cost and complexity, phantom-bit technology (PBT) is widely applicable in practical engineering [2]. Although PBT can improve seeker beam scanning accuracy, the beam pointing error appears because of the seeker using open-loop control to achieve beam pointing control. This fluctuates as beam scanning angle increases and causes incomplete missile body movement decoupling during seeker beam scanning. Here, another parasitic loop in the guidance loop appears. The incomplete decoupling effect of missile body motion caused by radome error and beam pointing error is known as the disturbance rejection effect (DRE) problem. The stability and precision of the missile guidance loop and the method of obtaining high accuracy LOS angular rate under the influence of DRE problem are worth noting.

The associate editor coordinating the review of this manuscript and approving it for publication was Sara Dadras.

Ehrich decoupled the guidance information from the body disturbance using the feedforward of the angular rate of the missile body [3]. Zarchan and Nesline emphasize the importance of the influence of the DRE parasitic loop induced by radome slope distortion on the guidance loop [4]. They also proposed a constant rate of compensation to slow down guidance and autopilot responses to decrease miss distance [5], [6]. Willman stated that unconformity between the beam control unit of the phased array radar seeker and the rate gyroscope would produce the DRE problem [7]. Bai et al. provide in-depth analysis of the work of the parasitic loop in the guidance loop induced by the DRE problem on the gimbal phased array seeker and the influence of missile body disturbance on the seeker performance [8]. Lu et al. analyzed the effect of the phased array seeker with PBT for the missile detection and guidance system [2]. According to the antenna element shift phase, they analyzed the antenna element shift phase law and the causes of beam pointing error under phantom-bit conditions. Zheng et al. studied the dynamic stability of the radar homing rolling missile with a two-loop autopilot and investigated the influence of the parasitic loop on the rolling missile guidance and control system [9]. They also analyzed the dynamic stability of rolling missiles with respect to the parasitic effect induced by the radome error slope [10]. Building on the research of Zheng et al., Tian et al. studied the dynamic stability of rolling missiles with three-loop autopilot [11]. Li et al. analyzed the stability of spinning missiles with respect to the disturbance induced by the DRE parasitic loop in the pitch and yaw channel [12]. Overall, these studies highlight the devastating influence of the DRE parasitic loop on the missile guidance system.

Compensation approaches needed to be determined after the DRE problem had been studied. Several kinds of DRE compensation approach have been suggested in the literature. The first approach is hardware based, meaning the careful manufacture of the radome and using a large amount of digital shifter in the seeker. The second approach is to measure and compensate, which means radome boresight error and beam pointing error measure and compensation. Further, the radome boresight error slope and beam pointing error slope can also be measured and compensated. The third approach is algorithmic, which means using control theory to slow down the guidance loop response or using the filter, such as the Kalman filter and its variants, to estimate the radome error slope and beam pointing error slope.

Various methods have been employed for estimation and compensation of the DRE parasitic loop. Wen et al. proposed a beam pointing error compensation method using PBT [13]. Dowling et al. designed a radome computer compensation method to mitigate the radome effect [14]. Building on the work of Dowling et al., a study by Das involved another method to address the continuous measurement error slope during radome fabrication [15]. In that method, the particular radome-antenna combination appeared unique. If any one of them changed, the measurement of the radome antenna combination should be changed too. In another major study, Klein et al. found that the loop-shaping approach could mitigate the radome effect [16]. They added a notch network in the parasitic loop to identify the frequency that causes a negative gain margin and to damp it. In a study investigating the DRE parasitic loop induced by the radome error and beam pointing error, Zong et al. reported that regarding the radome error and beam pointing error as a whole error and using the extended Kalman filter (EKF)to estimate and compensate it is a useful way to mitigate the DRE problem [17]. But in practice, the beam pointing error sometimes needs to be estimation and compensation independently. In a comprehensive study of the DRE parasitic loop in the gimbal phased array seeker, Hu et al. found that a strong tracking unscented Kalman filter (STUKF) can be used to estimate the DRE parasitic loop and compensate it in the guidance loop [18]. In nowadays more and more missiles contain strapdown phased array seeker that will challenge the performance of STUKF.

Most studies of the DRE parasitic loop have only focused on radome errors. A few compensation methods that take into account the beam pointing error slope tend to treat the radome error slope and the beam pointing error slope as a whole. It is well known that the radome error and beam pointing error have continuous nonlinearity in engineering practice. Thus, DRE parasitic loops caused by radome error and beam pointing error are nonlinear functions. In a study conducted by Bai *et al.* [19], the principal limitation of some experimental approaches, such as the robust Kalman filter [20] or unscented Kalman filter [21], [22], is that they are not good methods for solving nonlinear problems in practice. That is the main limitation of widely used filter techniques currently. Although studies have recognized the DRE parasitic loop, research has yet to systematically investigate the effects of DRE parasitic loops that independently consider radome error and beam pointing error, and estimation and compensation methods for this parasitic loop. Therefore, in this paper, the radome error and beam pointing error in the DRE parasitic loop are considered independently. Also, this paper set out to investigate the usefulness of a new estimation and compensation method using extended state Kalman filter (ESKF) in deal with the DRE parasitic loop in the missile guidance loop. The ESKF has the best performance among the performance comparison of ESKF, STUKF, and EKF. The proposed method can estimate two error slope accurately. Then it can output stable and accurate LOS angular rate. That is friendly to the guidance system and will help the missile to hit the target more precisely in the end.

This paper describes the design and implementation of a novel online estimation and compensation method for strapdown phased array radar seekers using ESKF. The benefit of this method is that stability of the filter is guaranteed for radome error slope and beam pointing error slope change with strong nonlinearity or have large initial estimation error and large noise. This paper has been divided into four sections. In the first section, the basic missile-target geometry model of the strapdown phased array radar seeker is established. According to this model, the DRE parasitic loop can be

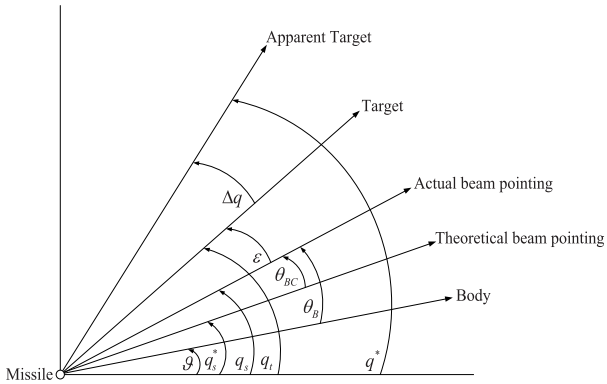

FIGURE 1. The basic missile-target geometry model of strapdown phased array radar seeker.

TABLE 1. The nomenclature of the DRE model.

q_t	The true LOS angle
$\dot{q}_s$	The LOS angular rate
q^*	The apparent LOS angle
θ_B	The beam pointing angle
θ_{BC}	The beam pointing angle instruction
ϵ	The tracking error angle
$\dot{\vartheta}$	The body moving rate
ϑ	The attitude angle.

constructed. Subsequently, the cause of the DRE problem and the influence on the guidance loop are analyzed. The analysis reveals that the beam pointing error and the radome error should both be as small as possible to guarantee the system is stable. The second section introduces the ESKF and its design process. By using the ESKF, an online estimation and compensation method for the DRE parasitic loop is established. The third section contains the numerical simulations among the EKF, the STUKF, and the proposed method. A more accurate LOS angular rate can be obtained using the proposed method which can raise the missile guidance loop stability and decrease the final miss distance. The final section summarizes the main findings of this paper.

A. MATHEMATICAL MODEL

The basic missile-target geometry is shown in Fig. 1.

According to Fig. 1, the nomenclature of DRE model is shown in Table. 1.

The apparent LOS angle q^* can be expressed as,

$$q^* = q_t + (q_s - \vartheta) R \tag{1}$$

In the stable tracking situation, the tracking error angle ϵ can be ignored and the radome error slope R is far less than 1 in practice. Hence, Eq.(1) can be substituted into

$$q^* \cong q_t + (q_t - \vartheta) R = q_t (1 + R) - \vartheta R = q_t - \vartheta R \tag{2}$$

Based on Fig. 1 and Eq.(2), the guidance loop can be obtained in Fig. 2.

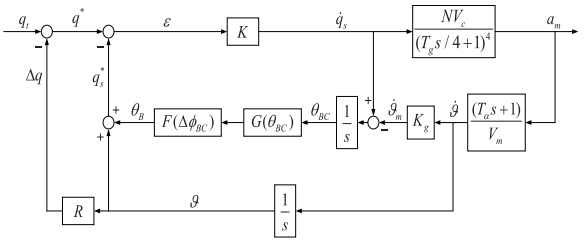

FIGURE 2. The block diagram of the guidance loop.

TABLE 2. The nomenclature of the guidance loop.

K	The strapdown phased array radar seeker forward loop gain
K_g	the angular rate gyro scale
T_α	The turning rate time constant of missile maneuverability
T_g	The approximate time constant of the guidance system
N	The effective navigation ratio
V_c	The closing velocity
V_m	The missile velocity
a_m	The acceleration of the missile
R	The radome error slope
$F(\Delta\phi_{BC})$ $G(\theta_{BC})$	The beam control unit
$\Delta\phi_{BC}$	the radiating element phase shift value.

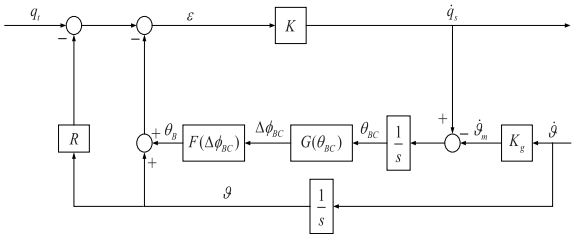

FIGURE 3. The block diagram of DRE parasitic loop.

The nomenclature of the guidance loop is shown in Table. 2.

In the missile guidance loop, the radome error slope R and the beam pointing error slope R^* can form two parasitic loops. These parasitic loops will both decrease the performance of the missile guidance system because of coupling with the missile body motion. In this paper, these parasitic loops are regarded as a single parasitic loop named the DRE parasitic loop. The block diagram of the DRE parasitic loop induced by radome error slope R and beam pointing error slope R^* is shown in Fig. 3.

According to the beam control principle [2], design $\Delta\theta = R^*\theta_{BC}$, then $\theta_B = (1 + R^*)\theta_{BC}$. Moreover, the angular rate gyro scale K_g in the missile high-precision inertial navigation system has a small fluctuation range (and can be controlled within the range of 10^{-3} during the whole flight), which means $K_g \cong 1$. Thus, Fig. 3 can be simplified to Fig. 4.

The LOS angular rate $\dot{q}_s$ can be influenced by body motion. Thus, from Fig. 4 the LOS angular rate $\dot{q}_s$ can be

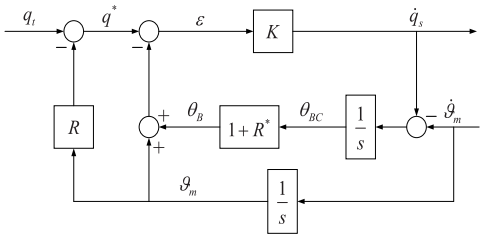

FIGURE 4. The block diagram of simplified DRE parasitic loop.

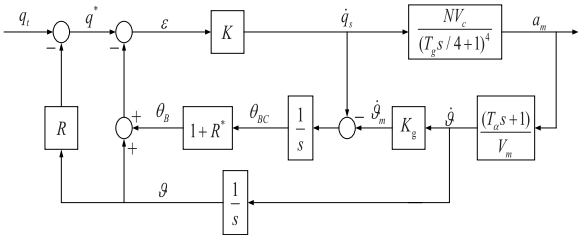

FIGURE 5. The block diagram of the guidance loop with DRE parasitic loop.

expressed as,

$$\dot{q}_s = \frac{K\dot{q}_t - K\dot{\vartheta}R + K\left(1+R^*\right)\dot{\vartheta} - K\dot{\vartheta}}{s+K\left(1+R^*\right)} \tag{3}$$

$$= \dot{q}_t\left(\frac{K}{s+K\left(1+R^*\right)}\right) + \dot{\vartheta}\left(\frac{K\left(1+R^*\right)-KR-K}{s+KG_\theta}\right), \tag{4}$$

and the component induced by body motion $\Delta\dot{q}_s$ is

$$\Delta\dot{q}_s = \dot{\vartheta}\left(\frac{K\left(1+R^*\right)-KR-K}{s+K\left(1+R^*\right)}\right) \tag{5}$$

that is

$$\frac{\Delta\dot{q}_s}{\dot{\vartheta}} = \frac{\left(1+R^*\right)-R-1}{\frac{s}{K}+\left(1+R^*\right)} \tag{6}$$

Thus, the DRE function can be expressed as,

$$G_{DRR} = \frac{R^*-R}{\frac{s}{K}+R^*+1} \tag{7}$$

From the DRE function Eq.(7), it is clear that the DRE problem is related to radome error slope R and beam pointing error slope R^*. Furthermore, the DRE problem exists when the equation $R^*-R=0$ holds.

To further illustrate the impact of the DRE parasitic loop in the missile guidance system, Fig. 2 is substituted into the missile guidance loop to obtain Fig. 5.

According to Fig. 5, the following closed-loop transfer function and characteristic equation can be obtained in Eq.(8) and Eq.(9) respectively.

$$H_{cl}(s) = \frac{a_m}{\dot{q}_t} = \frac{NV_c}{\left(\frac{s}{K}+1+R^*\right)\left(\frac{T_g}{4}s+1\right)^4 + \left(R^*-R\right)\frac{NV_c}{V_m}\left(T_\alpha s+1\right)} \tag{8}$$

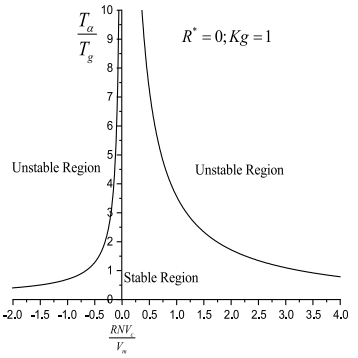

(a) The stable region when $R^*=0$

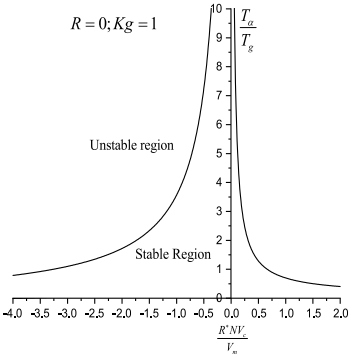

(b) The stable region when $R=0$

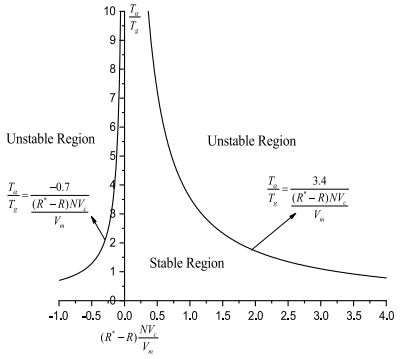

(c) The stable region with increasing $(R*-R)$

FIGURE 6. The stable region of the guidance loop with DRE parasitic loop.

$$\Phi(s) = \frac{NV_c}{\left(\frac{s}{K}+1+R^*\right)\left(\frac{T_g}{4}s+1\right)^4 + \left(R^*-R\right)\frac{NV_c}{V_m}\left(T_\alpha s+1\right)}. \tag{9}$$

Define $K=10$ and $N=4$ based on the freezing coefficient analysis method [23]. According to the Routh criterion [24], the stable region can be obtained in Fig. 6.

From Fig. 6, both the radome error slope R and the beam pointing error slope R^* have an effect on the parasitic loop stability region. The larger the absolute value of the total error slope R^*-R, the smaller the parasitic loop stability region. Also, the negative feedback stability region is larger than the positive feedback stability region. However, the mechanism of negative feedback caused by radome error

and beam pointing error is different. When the radome error slope is negative, negative feedback is generated. When the beam pointing error slope is positive, negative feedback is generated.

According to the above analysis, the existence of the DRE parasitic loop in the full strapdown phased array radar seeker can have a catastrophic influence on the missile guidance accuracy, resulting in miss distance increases or even divergence.

II. DESIGN THE ONLINE ESTIMATION AND COMPENSATION METHOD FOR DRE PARASITIC LOOP

A. ESKF DESIGN

Consider the following class of nonlinear time-varying uncertain systems,

$$\begin{cases} X_{k+1} = \bar{A}_k X_k + \bar{B}_k F(X_k, k) + w_k, \\ Z_k = \bar{C}_k X_k + n_k, \quad k = 0, 1, \ldots, \end{cases} \tag{10}$$

where $X_k \in \mathbb{R}^n$ is the state, $\bar{A}_k, \bar{B}_k$ and $\bar{C}_k$ are known time-varying matrixes with $\bar{A}_k \in \mathbb{R}^{n\times n}, \bar{B}_k \in \mathbb{R}^{n\times l}, \bar{C}_k \in \mathbb{R}^{m\times n}$. $F(X_k, k) \in \mathbb{R}^l$ is the nonlinear uncertain dynamics in the system, and its nominal model is the known function $\bar{F}(X_k, k)$. $w_k \in \mathbb{R}^n$ and $n_k \in \mathbb{R}^m$ are the process noise and measurement noise, respectively. $Z_k \in \mathbb{R}^m$ is the measurement output.

Remark 1: $F(X_k, k)$ is usually referred to as the "total disturbance" lumping both internal uncertain dynamics and external disturbance, such as the unknown parameter variations, the unmodeled dynamics, and the discretization errors [25].

In model, the uncertain dynamics are divided into three parts: the known linear part $\bar{A}_k X_k$, the time-varying nonlinear uncertain dynamics $F(X_k, k)$, and the noise (w_k, n_k). The ESKF filter method suggested using different methods to deal with different kinds of uncertainties. $F(X_k, k)$ is treated as an extended state to be estimated as well as compensated for, and (w_k, n_k) is attenuated by the optimization technique of the Kalman filter. Therefore, the system can be equivalently transformed to,

$$\begin{cases} \begin{bmatrix} X_{k+1} \\ F_{k+1} \end{bmatrix} = \mathbf{A}_k \begin{bmatrix} X_k \\ F_k \end{bmatrix} + \mathbf{B}_k G_k + \begin{bmatrix} w_k \\ 0 \end{bmatrix}, \\ Z_k = \mathbf{C}_k \begin{bmatrix} X_k \\ F_k \end{bmatrix} + n_k, \end{cases} \tag{11}$$

where

$$F_k \triangleq F(X_k, k), \quad G_k = F_{k+1} - F_k,$$
$$\mathbf{A}_k = \begin{bmatrix} \bar{A}_k & \bar{B}_k \\ 0 & I \end{bmatrix}, \quad \mathbf{B}_k = \begin{bmatrix} 0 \\ I \end{bmatrix}, \ \mathbf{C}_k = \begin{bmatrix} \bar{C}_k & 0 \end{bmatrix}.$$

For the following construction process, there are four assumptions that need to be known.

Assumption 1: $(\mathbf{A}_k, \mathbf{C}_k)$ is uniformly observable.

Assumption 2: $\{w_k\}_0^\infty$ and $\{n_k\}_0^\infty$ are uncorrelated zero-mean Gaussian random sequences and $E(n_k n_k^T) \le R_k, E(w_k w_k^T) \le S_k$, where $\{R_k\}_{k=0}^\infty$ and $\{S_k\}_{k=0}^\infty$ are known and uniformly bounded. In addition, $\{w_k\}_0^\infty$, $\{n_k\}_0^\infty$ and X_0 are mutually independent.

Assumption 3:

$$E\left(\begin{bmatrix} X_0 - \hat{X}_0 \\ F_0 - \hat{F}_0 \end{bmatrix} \begin{bmatrix} X_0 - \hat{X}_0 \\ F_0 - \hat{F}_0 \end{bmatrix}^T\right) \le \mathbf{P}_0 \tag{12}$$

where $\hat{X}_0$ is the estimate of X_0, $\hat{F}_0 \triangleq \bar{F}(\hat{X}_0, 0)$ and P_0 is a known constant matrix.

Assumption 4:

$$E(G_{k,i}^2) \le \bar{q}_{k,i}, \quad i = 1, 2, \ldots \tag{13}$$

where $\{\bar{q}_{k,i}\}_{k=0}^\infty$ is known and uniformly bounded.

Remark 2: $\bar{q}_k$ represents the size of the varying of the nonlinear uncertainty $F(\cdot)$. Besides, the upper bounds P_0 and $\bar{q}_k$ can be chosen according to the priori information of the sensors and physical limitations on the practical systems.

Design of ESO based on the extended model in Eq.(11).

$$\begin{bmatrix} \hat{X}_{k+1} \\ \hat{F}_{k+1} \end{bmatrix} = \mathbf{A}_k \begin{bmatrix} \hat{X}_k \\ \hat{F}_k \end{bmatrix} + \mathbf{B}_k \hat{G}_k - K_k \left(Z_k - \mathbf{C}_k \begin{bmatrix} \hat{X}_k \\ \hat{F}_k \end{bmatrix} \right), \tag{14}$$

here, $\hat{G}_k$, the estimate of G_k, is used to correct the estimation error of the state and the uncertainty by making full use of the model information. Thus, using the nominal model of G_k, $\bar{G}_k = \bar{F}(X_{x+1}, k+1) - \bar{F}(X_k, k)$. Then the estimate of is denoted as $\hat{\bar{G}}_k = \bar{F}(\bar{A}_k \hat{X}_k + \bar{B}_k \hat{F}_k, k+1) - \bar{F}(X_k, k)$. According to the estimate of the nominal model $\bar{G}_k$, $\hat{G}_k$ is designed as $\hat{G}_{k,i} = sat\left(\hat{\bar{G}}_{k,i}, \sqrt{\bar{q}_{k,i}}\right), \ i = 1, 2, \ldots,$ where $sat(\cdot)$ is the saturation function defined by $sat(f, b) = \max\{\min\{f, b\}, -b\}, \quad b > 0$. The saturation function $sat(\cdot)$ is used to ensure the boundedness of $\hat{G}_{k,i}$. According to the Young's inequality for the matrices case and Assumption 4, we can obtain,

$$\begin{aligned} &\left(G_k - \hat{G}_k\right)\left(G_k - \hat{G}_k\right)^T \\ &\le 2G_k G_k^T + 2\hat{G}_k \hat{G}_k^T \\ &\le 2l\,\mathrm{diag}\left(\left[G_{k,1}^2 G_{k,2}^2 \cdots G_{k,l}^2\right]\right) \\ &\quad + 2l\,\mathrm{diag}\left(\begin{bmatrix} \hat{G}_{k,1}^2 & \hat{G}_{k,2}^2 & \cdots & \hat{G}_{k,l}^2 \end{bmatrix}\right) \\ &\le 4l\,\mathrm{diag}\left(\begin{bmatrix} \bar{q}_{k,1} & \cdots & \bar{q}_{k,l} \end{bmatrix}\right), \end{aligned}$$

then

$$\mathbf{Q}_{1,k} = \begin{bmatrix} 0_{n\times n} & 0_{n\times l} \\ 0_{l\times n} & 4\bar{\mathbf{Q}}_k \end{bmatrix}, \tag{15}$$

where $\bar{\mathbf{Q}}_k \triangleq l \cdot \mathrm{diag}\left(\begin{bmatrix} \bar{q}_{k,1} & \bar{q}_{k,2} & \cdots & \bar{q}_{k,l} \end{bmatrix}\right)$.

Design θ to decouple the cross terms of estimation error and the uncertainties.

$$\theta = \sqrt{\frac{tr\left(Q_{1,0}\right)}{tr\left(P_0\right)}}, \tag{16}$$

and

$$\mathbf{Q}_{2,k} = \begin{bmatrix} S_k & 0_{n\times l} \\ 0_{l\times n} & 0_{l\times l} \end{bmatrix}. \tag{17}$$

From Assumption 2 we have

$$\begin{bmatrix} E\left(w_k w_k^T\right) & 0_{n\times l} \\ 0_{l\times n} & 0_{l\times l} \end{bmatrix} \le \mathbf{Q}_{2,k}, \tag{18}$$

let $\mathbf{P}_k$ satisfy the following iteration equation,

$$\begin{aligned}\mathbf{P}_{k+1} = {} & (1+\theta)\left(\mathbf{A}_k + K_k\mathbf{C}_k\right)\mathbf{P}_k\left(\mathbf{A}_k + K_k\mathbf{C}_k\right)^T \\ & + K_k R_k K_k^T + \left(1+\frac{1}{\theta}\right)\mathbf{Q}_{1,k} + \mathbf{Q}_{2,k},\end{aligned} \tag{19}$$

with the initial value $\mathbf{P}_0$.

Define

$$\begin{aligned}K_k^* = \arg\min_{K_k}\Big\{ & (1+\theta)\left(\mathbf{A}_k + K_k\mathbf{C}_k\right)\mathbf{P}_k\left(\mathbf{A}_k + K_k\mathbf{C}_k\right)^T \\ & + K_k R_k K_k^T\Big\},\end{aligned}$$

Since $\mathbf{P}_k$ is a positive semi-definite matrix and R_k is a positive definite matrix, $\mathbf{C}_k\mathbf{P}_k\mathbf{C}_k^T + \frac{1}{1+\theta}R_k$ is positive definite. It is straightforward to obtain,

$$K_k^* = -\mathbf{A}_k\mathbf{P}_k\mathbf{C}_k^T\left(\mathbf{C}_k\mathbf{P}_k\mathbf{C}_k^T + \frac{1}{1+\theta}R_k\right)^{-1}. \tag{20}$$

Subsequently, the gain matrix K_k of the estimator is optimized timely based on the prior information Assumption 2-Assumption 4. As a consequence, the ESKF can be designed as follows:

$$\begin{bmatrix}\hat{X}_{k+1}\\ \hat{F}_{k+1}\end{bmatrix} = \mathbf{A}_k\begin{bmatrix}\hat{X}_k\\ \hat{F}_k\end{bmatrix} + \mathbf{B}_k\hat{G}_k - K_k\left(Z_k - \mathbf{C}_k\begin{bmatrix}\hat{X}_k\\ \hat{F}_k\end{bmatrix}\right), \tag{21}$$

$$K_k = -\mathbf{A}_k P_k\mathbf{C}_k^T\left(\mathbf{C}_k\mathbf{P}_k\mathbf{C}_k^T + \frac{1}{1+\theta}R_k\right)^{-1}, \tag{22}$$

$$\begin{aligned}\mathbf{P}_{k+1} = {} & (1+\theta)\left(\mathbf{A}_k + K_k\mathbf{C}_k\right)\mathbf{P}_k\left(\mathbf{A}_k + K_k\mathbf{C}_k\right)^T, \\ & + K_k R_k K_k^T + \left(1+\frac{1}{\theta}\right)\mathbf{Q}_{1,k} + \mathbf{Q}_{2,k}.\end{aligned} \tag{23}$$

where

$$\begin{aligned}\mathbf{Q}_{1,k} &= \begin{bmatrix}0_{n\times n} & 0_{n\times l}\\ 0_{l\times n} & 4\bar{\mathbf{Q}}_k\end{bmatrix},\\ \mathbf{Q}_{2,k} &= \begin{bmatrix}\mathbf{S}_k & 0_{n\times l}\\ 0_{l\times n} & 0_{l\times l}\end{bmatrix},\\ \bar{\mathbf{Q}}_k &\triangleq l\cdot\mathrm{diag}\left(\begin{bmatrix}\bar{q}_{k,1} & \bar{q}_{k,2} & \cdots & \bar{q}_{k,l}\end{bmatrix}\right),\\ \theta &= \sqrt{\frac{tr\left(Q_{1,0}\right)}{tr\left(P_0\right)}},\\ \hat{G}_{k,i} &\triangleq \mathrm{sat}\left(\bar{G}_{k,i}, \sqrt{\bar{q}_{k,i}}\right),\\ \bar{G}_k &\triangleq \bar{G}\left(\hat{X}_k, k\right),\\ \mathrm{sat}\left(f, b\right) &= \max\left\{\min\left\{f, b\right\}, -b\right\}, b > 0.\end{aligned}$$

For the system with uncertainty and noise, the tuning of K_k becomes a tradeoff between the disturbance rejection and the noise sensitivity. This is because higher K_k leads to faster tracking, but also results in higher levels of noise. Thus, different from ESO, K_k is no longer static and manually tuned here. Instead, K_k is optimized to ensure the mean square estimation error is minimal at each step. For more details about ESKF, please refer to [19].

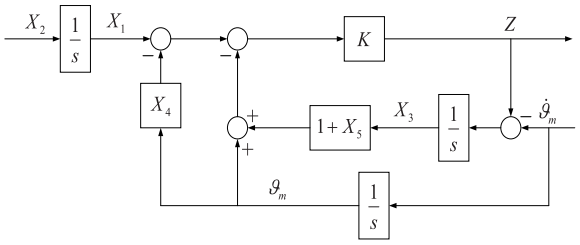

FIGURE 7. The block diagram of the ESKF model for DRE parasitic loop.

B. ONLINE ESTIMATION AND COMPENSATION METHOD FOR DRE PARASITIC LOOP BASED ON ESKF FILTER

The beam pointing error slope R^* and the radome error slope R (which affect the DRE parasitic loop of the strapdown phased array radar seeker) are set as the state variables. The beam pointing error slope estimate value $\hat{R}^*$, the radome error slope estimate value $\hat{R}$, and the true LOS angular rate estimate value $\hat{\dot{q}}_t$ are directly obtained with the ESKF filter. Thereby, the online compensation for the DRE parasitic loop is completed.

Setting the system state variables of the ESKF filter to

$$\mathbf{X} = \left[X_1, X_2, X_3, X_4, X_5\right]^T = \left[q_t, \dot{q}_t, \theta_B, R, R^*\right]^T, \tag{24}$$

The LOS angular rate $\dot{q}_s$ is a measured output and is expressed as,

$$Z = \dot{q}_s. \tag{25}$$

The attitude angle ϑ_m and the attitude angular rate $\dot{\vartheta}_m$ are measured by the inertial navigation system onboard the missiles. They are the input quantities for the ESKF, the corresponding noise standard deviations are σ_{u1} and σ_{u2}, respectively. Thus, the ESKF model for the DRE parasitic loop can be obtained in Fig. 5.

According to Fig. 5, the state equation and the measurement equation of the ESKF filter are obtained as follows,

$$\dot{\mathbf{X}}(t) = f[\mathbf{X}(t)] + \mathbf{m}\mathbf{w}(t), \tag{26}$$

$$\mathbf{Z}(t) = h[\mathbf{X}(t)] + \mathbf{v}(t), \tag{27}$$

where,

$$f[\mathbf{X}(t)] = \begin{bmatrix} X_2 \\ 0 \\ K\mathbf{X}_1 - K\vartheta_m - K\mathbf{X}_5\vartheta_m - K\mathbf{X}_3 - K\mathbf{X}_3\mathbf{X}_4 - \dot{\vartheta}_m \\ 0 \\ 0 \end{bmatrix},$$

$$h[\mathbf{X}(t)] = K\mathbf{X}_1 - K\mathbf{X}_5\vartheta_m - K\mathbf{X}_3 - K\mathbf{X}_3\mathbf{X}_4 - K\vartheta_m - \dot{\vartheta}_m,$$

$$\mathbf{w}(t) = \begin{bmatrix}0 & w_2(t) & 0 & w_4(t) & w_5(t)\end{bmatrix}^T.$$

$f[\mathbf{X}(t)]$ represents the state matrix and $h[\mathbf{X}(t)]$ represents the measurement matrix. $\mathbf{w}(t)$ and $\mathbf{v}(t)$ are the precess noise and measurement noise, respectively. Design S_{w2}, S_{w4} and S_{w5} are the process noise power spectral densities. $\mathbf{S}_k$ is the system noise covariance matrix. $\mathbf{v}(t)$ is the zero-mean Gauss white-noise and its standard deviation is represented as σ_v. $\mathbf{R}_k$ is the measurement noise covariance matrix.

According to the ESKF design process Eq.(11) described in Section II-A, the nonlinear uncertain dynamics F_k can be set as

$$F_k = \begin{bmatrix} \dot{R} \\ \dot{R}^* \end{bmatrix}, \tag{28}$$

then the state equation and measurement equation can be substituted as shown in Eq.(29), as shown at the bottom of this page, where Δt is sample time. Then, the discrete fundamental matrix $\bar{\mathbf{A}}[\hat{\mathbf{X}}(t)]$ is shown in Eq.(30), as shown at the bottom of this page, the disturbance matrix $\bar{\mathbf{B}}\left[\hat{\mathbf{X}}(t)\right]$ and the discrete measurement matrix $\bar{\mathbf{C}}\left[\hat{\mathbf{X}}(t)\right]$ are obtained in Eq.(31) and Eq.(32), respectively.

$$\bar{\mathbf{B}}\left[\hat{\mathbf{X}}(t)\right] = \begin{bmatrix} 0 & 0 \\ 0 & 0 \\ 0 & 0 \\ 0 & 0 \\ 0 & 0 \\ 1 & 0 \\ 0 & 1 \end{bmatrix}, \tag{31}$$

$$\bar{\mathbf{C}}\left[\hat{\mathbf{X}}(t)\right] = \begin{bmatrix} K & 0 & K - K\mathbf{X}_{4,k/k-1} & K\mathbf{X}_{3,k/k-1} & K\vartheta & 0 & 0 \end{bmatrix}. \tag{32}$$

The unknown disturbance nominal matrix $\mathbf{G}_k$ can be written as,

$$\mathbf{G}_k = \begin{bmatrix} \dot{R} + w_4(k) \\ \dot{R}^* + w_5(k) \end{bmatrix}. \tag{33}$$

The ESO method is applied to estimate and compensate the unknown disturbance. Hence, the nominal model of $\mathbf{G}_k$ is used as,

$$\bar{\mathbf{G}}_k = \begin{bmatrix} \mathbf{X}_{4,k} - \hat{\mathbf{X}}_{4,k-1} \\ \mathbf{X}_{5,k} - \hat{\mathbf{X}}_{5,k-1} \end{bmatrix}. \tag{34}$$

The extended model disturbance estimation covariance matrix $\mathbf{Q}_{1k}$ is

$$\mathbf{Q}_{1k} = \begin{bmatrix} 0_{5\times5} & 0_{5\times2} \\ 0_{2\times5} & \bar{\mathbf{Q}}_k \end{bmatrix}, \tag{35}$$

where

$$\bar{\mathbf{Q}}_k = 4 \times 2 \times \begin{bmatrix} R_{k+1} + w_{4,k+1} - R_k - w_{4,k} & 0 \\ 0 & R^*_{k+1} + w_{5,k+1} - R^*_k - w_{5,k} \end{bmatrix},$$

and the design of the extended model noise covariance matrix $\mathbf{Q}_{2k}$ is:

$$\mathbf{Q}_{2k} = \begin{bmatrix} 0 & 0 & 0 & 0 & 0 & 0 & 0 \\ 0 & \frac{S_{w2,k-1}}{\Delta t} & 0 & 0 & 0 & 0 & 0 \\ 0 & 0 & 0 & 0 & 0 & 0 & 0 \\ 0 & 0 & 0 & \frac{S_{w4,k-1}}{\Delta t} & 0 & 0 & 0 \\ 0 & 0 & 0 & 0 & \frac{S_{w5,k-1}}{\Delta t} & 0 & 0 \\ 0 & 0 & 0 & 0 & 0 & 0 & 0 \\ 0 & 0 & 0 & 0 & 0 & 0 & 0 \end{bmatrix}. \tag{36}$$

$$\begin{cases} \mathbf{X}_{k+1} = \begin{bmatrix} 1 & \Delta t & 0 & 0 & 0 \\ 0 & 1 & 0 & 0 & 0 \\ K\Delta t & 0 & 1 - K\Delta t - K\hat{\mathbf{X}}_4\Delta t & -K\hat{\mathbf{X}}_3\Delta t & -K\vartheta_m\Delta t \\ 0 & 0 & 0 & 1 & 0 \\ 0 & 0 & 0 & 0 & 1 \end{bmatrix} \mathbf{X}_k \\ \qquad + \begin{bmatrix} 0 & 0 \\ 0 & 0 \\ 0 & 0 \\ \Delta t & 0 \\ 0 & \Delta t \end{bmatrix} \begin{bmatrix} \dot{R} \\ \dot{R}^* \end{bmatrix} + \mathbf{m}\mathbf{w}_k, \\ \mathbf{Z}_k = \begin{bmatrix} K & 0 & -K - K\hat{\mathbf{X}}_4 & -K\hat{\mathbf{X}}_3 & -K\vartheta_m \end{bmatrix} \hat{\mathbf{X}}_k + \mathbf{n}_k, \quad k = 0, 1, \ldots, \end{cases} \tag{29}$$

$$\bar{\mathbf{A}}[\hat{\mathbf{X}}(t)] = \begin{bmatrix} 1 & \Delta t & 0 & 0 & 0 & 0 & 0 \\ 0 & 1 & 0 & 0 & 0 & 0 & 0 \\ K\Delta t & 0 & 1 - K\Delta t - K\hat{\mathbf{X}}_{4,k-1}\Delta t & -K\hat{\mathbf{X}}_{3,k-1}\Delta t & -K\vartheta_m\Delta t & 0 & 0 \\ 0 & 0 & 0 & 1 & 0 & \Delta t & 0 \\ 0 & 0 & 0 & 0 & 1 & 0 & \Delta t \\ 0 & 0 & 0 & 0 & 0 & 1 & 0 \\ 0 & 0 & 0 & 0 & 0 & 0 & 1 \end{bmatrix}, \tag{30}$$

TABLE 3. The simulation parameters of DRE model.

Parameter	σ_v	σ_{u1}	σ_{u2}	S_{w2}	S_{w4}	S_{w5}
Value	$0.2°/s$	$0.1°$	$0.1°/s$	0.00001	0.001	0.001

Then the design of the discrete system noise driven covariance matrix of the extended model is

$$\Gamma_k \approx \mathbf{m} \cdot \Delta t = \begin{bmatrix} \Delta t & 0 & 0 & 0 & 0 \\ 0 & \Delta t & 0 & 0 & 0 \\ 0 & 0 & \Delta t & 0 & 0 \\ 0 & 0 & 0 & \Delta t & 0 \\ 0 & 0 & 0 & 0 & \Delta t \end{bmatrix}. \quad (37)$$

Furthermore, the design measurement noise covariance matrix of the extended model is

$$\mathbf{R}_k = \frac{S_v}{\Delta t} = (\sigma_v)^2. \quad (38)$$

Then the online estimation and compensation method for the DRE parasitic loop using ESKF (Eqs. (21)-(23)) is designed as follows,

$$\begin{aligned} K_k &= -\bar{\mathbf{A}}_k \mathbf{P}_k \bar{\mathbf{C}}_k^T \left(\bar{\mathbf{C}}_k \mathbf{P}_k \bar{\mathbf{C}}_k^T + \frac{1}{\Delta t + \theta} \mathbf{R}_k \right)^{-1}, \\ \mathbf{P}_{k+1} &= (\Delta t + \theta) \left(\bar{\mathbf{A}}_k + K_k \bar{\mathbf{C}}_k \right) \mathbf{P}_k \left(\bar{\mathbf{A}}_k + K_k \bar{\mathbf{C}}_k \right)^T \\ &\quad + K_k \mathbf{R}_k K_k^T + \left(1 + \frac{1}{\theta} \right) \mathbf{Q}_{1,k} + \Gamma_k \mathbf{Q}_{2,k} \Gamma_k^T. \end{aligned} \quad (39)$$

III. MATHEMATICAL SIMULATION AND RESULT ANALYSIS

A. PARASITIC LOOP SIMULATION

In this section, the ESKF method is applied to achieve online estimation and compensation for the DRE parasitic loop by estimating the radome error slope R, beam pointing error slope R^*, and the LOS angular rate $\dot{q}_t$. The simulation parameters are designed in Table 3.

The strapdown phased array radar seeker forward loop gain was set to $K = 10$. The actual LOS angle was set as $q_t = 1t°$. Consequently, the LOS angular rate is $\dot{q}_t = 1°/s$. Also, it is assumed that the missile body motion varies sinusoidally with amplitude 3° and frequency of $2Hz$. The initial value of the state estimation was defined as $\hat{\mathbf{X}}_0 = [0,\ 0,\ 0,\ 0,\ 0]$, $\hat{\mathbf{F}}_0 = [0,\ 0]$, and the initial value of the extended model estimation error covariance matrix was set as $\mathbf{P}_0 = I_{7\times7}$. For simplicity, "ESKF" is used to represent the proposed method in the following simulations.

The method introduced in this paper has the same inputs as the traditional EKF. To reflect the robustness and higher estimation precision of the proposed method, selecting the EKF, which has been widely used in engineering practice, and the STUKF [18] as comparative items for the following simulation.

Firstly, it is assumed that the radome error slope and beam pointing error slope are $R = 0.06\sin(\pi t)$ and $R^* = 0.06\cos(\pi t)$, respectively. The result is shown in Fig. 8.

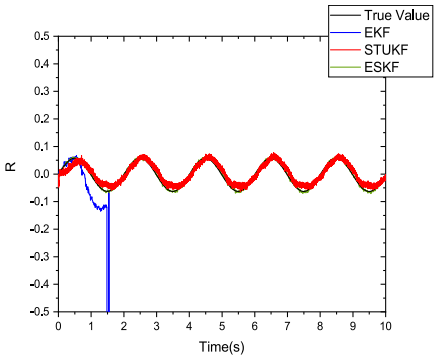

(a) The estimation of radome error slope R

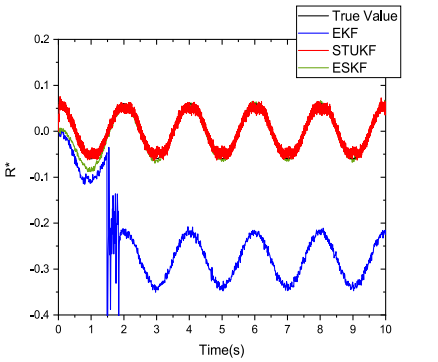

(b) The estimation of beam pointing error slope R^*

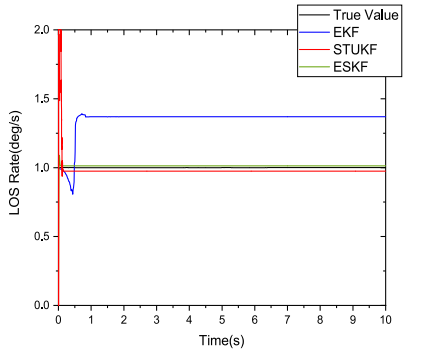

(c) The LOS angular rate output $\dot{q}_s$

FIGURE 8. The simulation results of ESKF, EKF and STUKF for the DRE parasitic loop.

As shown in Fig. 8(a) and (b), compared with the EKF, STUKF and ESKF can be used to estimate the beam pointing error slope and the radome error slope more accurately. This is because a singularity may occur with the EKF which results in divergence without the conditions of sufficient small noise. The ESKF can output a more smooth signal than STUKF, because the assistance of ESO. Under the large initial error condition, the STUKF and the proposed ESKF converge to the truth value in finite time. Then, Fig. 8(c) shows ESKF and STUKF both can compensate for the LOS angular rate more accurately in real-time than EKF. But with the large chattering in a small period start from the beginning, STUKF will harm the guidance loop. Moreover, ESKF is more accurate than STUKF. Thus, the DRE problem on the LOS angular rate output is well eliminated by ESKF.

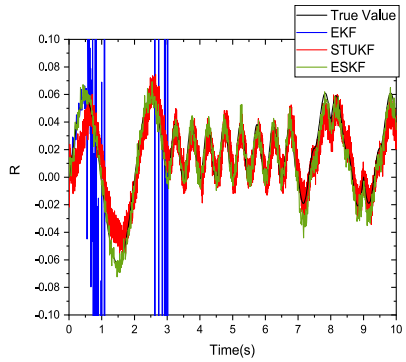

(a) The estimation of radome error slope R

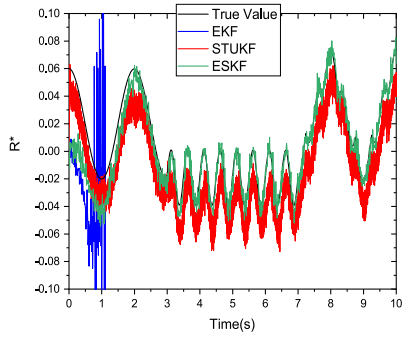

(b) The estimation of beam pointing error slope R^*

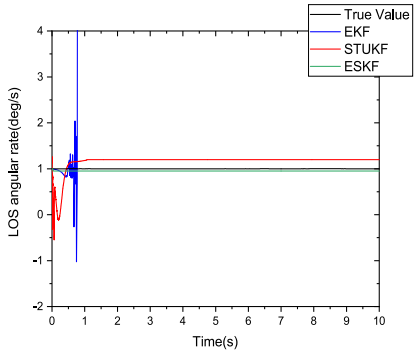

(c) The LOS angular rate output $\dot{q}_s$

FIGURE 9. The simulation results of ESKF, EKF and STUKF for the DRE parasitic loop.

Secondly, for the purpose of demonstrating the advantage of ESKF, a stronger nonlinear condition was used. The radome error slope R and beam pointing error slope R^* are given by:

$$\dot{R} = \begin{cases} 0.06\pi \cos(\pi t), & 0 \le t < 3, \\ 0.08\pi \sin(4\pi t), & 3 \le t < 7, \\ 0.06\pi \cos(3\pi t)\, \mathrm{sign}(\sin(2\pi t)), & 7 \le t < 10. \end{cases}$$

And,

$$\dot{R}^* = \begin{cases} -0.04\pi \sin(\pi t), & 0 \le t < 3, \\ 0.08\pi \cos(4\pi t), & 3 \le t < 7, \\ -0.06\pi \sin(3\pi t)\, \mathrm{sign}(\cos(2\pi t)), & 7 \le t < 10. \end{cases}$$

The simulation results are shown in Fig. 9.

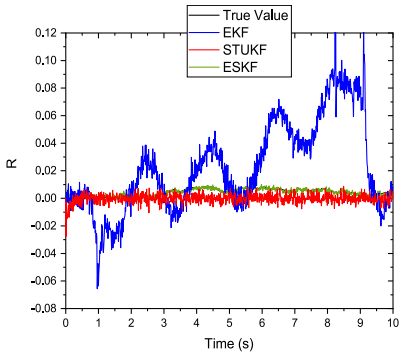

(a) The estimation of radome error slope R

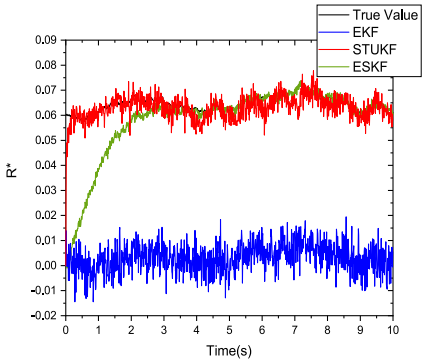

(b) The estimation of beam pointing error slope R^*

FIGURE 10. The simulation results of ESKF, EKF and STUKF for the DRE parasitic loop.

TABLE 4. The parameters of guidance loop withe DRE parasitic loop.

Parameter	K	N	V_c	V_m	T_α	T_g	ϵ
Value	10	4	1500 m/s	1000 m/s	1.2	0.4	5°

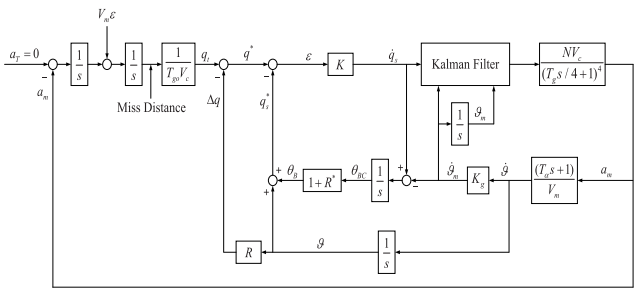

FIGURE 11. The block diagram of the missile guidance loop includes the Kalman filter.

Fig. 9(a) shows that the EKF performance decreases with the gradual increase of the nonlinearity. Also, the estimation accuracy decreases significantly and fluctuates greatly. This eventually results in bad LOS angular rate estimation and compensation. Fig. 9(b) shows that the STUKF can eliminate the initial error and estimate more accuracy than EKF. Unfortunately, there is a small error between the True Value and the STUKF. With the assistant of ESO, the ESKF can estimate the two error slopes throughout the entire flight time stably and accurately, even have a large initial error. This ensures a

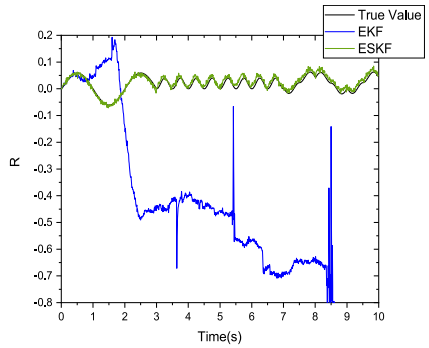

(a) The estimation of radome error slope R

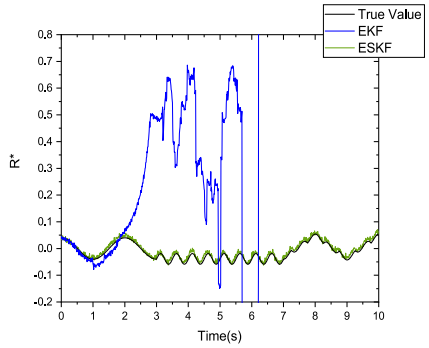

(b) The estimation of beam pointing error slope R^*

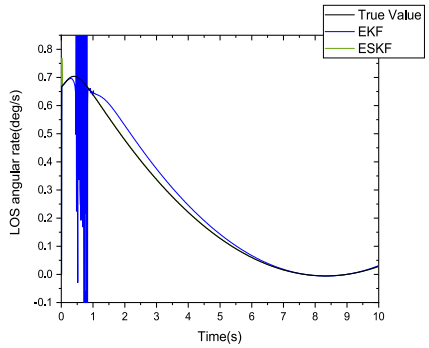

(c) The LOS angular rate output $\dot{q}_s$

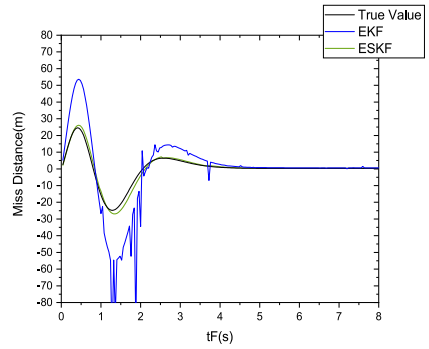

(d) The estimation of radome error slope R

FIGURE 12. The simulation results of ESKF filter and EKF filter for guidance loop.

high-precision estimate and compensates for the value of the LOS angular rate, which can be seen in Fig. 9(c).

Thirdly, considering the radome error slope R is a random value within the range of $(-0.03, 0.03)$ and the beam pointing error slope R^* is a random value in the range of $(-0.05, 0.05)$. This part of simulation is only looking for the EKF, STUKF and ESKF performance differences of the estimation of these two error slope. The simulation results are shown in Fig. 10.

As shown in Fig. 10(a), the performance of EKF is worst. The ESKF can estimate more accurate and more stable than STUKF under the small initial error condition. There is a initial estimation error using STUKF. Fig. 10(b) reveals that the ESKF cost more time to achieve a stable and precise estimation than low nonlinear condition. Although the STUKF can estimate fast, there still have a estimation error which cannot be ignored.

B. GUIDANCE LOOP SIMULATION

To verify the online compensation effect of the ESKF on the DRE parasitic loop for the full strapdown phased array radar seeker, the filter is applied to the missile guidance loop model. Because of the STUKF needs great amount of calculation, taking EKF as comparative item for better test the ESKF in engineering practice is enough in this section. The initial velocity pointing error input is taken as an example to complete the real-time online estimation of the beam pointing error slope, the radome error slope, and the LOS angular rate. Then the current estimated value of LOS angular rate is used to compensate the DRE parasitic loop in the full strapdown phased array radar seeker. Fig. 10 shows the block diagram of the missile guidance loop with a Kalman filter.

The parameters of the guidance loop were set in Table 4.

The simulation results are shown in Fig. 11.

Figures 11(a) and (b) show that in the guidance loop under the initial velocity pointing error input, the ESKF can estimate the seeker beam pointing error slope and the radome error slope more accurately than the EKF. Because of these accurate estimates, the ESKF can achieve excellent online compensation for the DRE parasitic loop. From Fig. 11(c), the ESKF performs more stably and accurately for the real-time online estimation of the LOS angular rate than the EKF. Moreover, Fig. 11(d) shows that since the EKF uses a singular value in estimating and compensating the LOS angular rate, it is not optimal for use in the guidance system. Missile guidance accuracy results in the miss distance fluctuating drastically. Overall, these results indicate that ESKF can estimate and compensate the LOS angular rate output value stably and provide accurate input values for the guidance law in real time. This is beneficial to the guidance system's ability to output accurate guidance commands and ensure the accuracy of the missile final hit.

IV. CONCLUSION

The purpose of this paper was to find a novel method using the ESKF to estimate and compensate the DRE parasitic loop in the guidance loop. The DRE parasitic loop has been shown to be caused by the radome error and beam pointing error in the guidance loop which in turn is caused by the missile body motion being coupled into the missile guidance loop. This affected the accuracy of the LOS angular rate output value and brought the unexpected DRE problem. The research has

also shown that the proposed method is used to estimating the radome error slope and the beam pointing error slope. Then using it to compensate LOS angular rate output value in real time. The results of mathematical simulations show that the proposed method can estimate the radome error slope and the beam pointing error slope more stably and accurately than the EKF and the STUKF. Additionally, it can compensate LOS angular rate output in real time and improve the missile guidance system accuracy and stability.

REFERENCES

[1] P. Zarchan, *Tactical and Strategic Missile Guidance*, 6th ed. Washington, DC, USA: American Institute of Aeronautics and Astronautics, 2012. [Online]. Available: http://arc.aiaa.org/doi/book/10.2514/4.868948

[2] T. Lu, Q. Wen, and J. Yin, "The effect of phantom-bit technology on the performance of phased array seeker detection in the case of the initial beam angle," *Optik*, vol. 127, no. 20, pp. 9996–10003, Oct. 2016. [Online]. Available: https://linkinghub.elsevier.com/retrieve/pii/S0030402616308646

[3] R. D. Ehrich and P. Vergez, "Strapdown seeker technology for the terminal guidance of tactical weapons," in *Proc. AGARD Guid. Control Aspects Tactical Air-Launched Missiles*, Oct. 1980, p. 15. [Online]. Available: http://adsabs.harvard.edu/abs/1980gcat.agar. . .e

[4] F. W. Nesline and P. Zarchan, "Missile guidance design tradeoffs for high-altitude air defense," *J. Guid., Control, Dyn.*, vol. 6, no. 3, pp. 207–212, May 1983. [Online]. Available: http://arc.aiaa.org/doi/10.2514/3.19817

[5] F. Nesline and P. Zarchan, "Radome induced miss distance in aerodynamically controlled homing missiles," in *Proc. Amer. Inst. Aeronaut. Astronaut.*, Jun. 1984, p. 1845. [Online]. Available: http://arc.aiaa.org/doi/10.2514/6.1984-1845

[6] F. W. Nesline, "Missile guidance for low-altitude air defense," *J. Guid. Control*, vol. 2, no. 4, pp. 283–289, Jul. 1979. [Online]. Available: http://arc.aiaa.org/doi/10.2514/3.55876

[7] W. W. Willman, "Effects of strapdown seeker scale-factor uncertainty on optimal guidance," *J. Guid., Control, Dyn.*, vol. 11, no. 3, pp. 199–206, May 1988. [Online]. Available: http://arc.aiaa.org/doi/10.2514/3.20294

[8] R. Bai, Q. Xia, and X. Du, "The study of guidance performance of a phased array seeker with platform," *Optik*, vol. 132, pp. 9–23, Mar. 2017. [Online]. Available: https://linkinghub.elsevier.com/retrieve/pii/S0030402616315728

[9] D. Zheng, D. Lin, J. Wang, and X. Xu, "Dynamic stability of rolling missiles employing a two-loop autopilot with consideration for the radome aberration parasitic feedback loop," *Aerosp. Sci. Technol.*, vol. 61, pp. 1–10, Feb. 2017. [Online]. Available: https://linkinghub.elsevier.com/retrieve/pii/S1270963816311269

[10] D. Zheng, D. Lin, X. Xu, and S. Tian, "Dynamic stability of rolling missile with proportional navigation& PI autopilot considering parasitic radome loop," *Aerosp. Sci. Technol.*, vol. 67, pp. 41–48, Aug. 2017. [Online]. Available: http://www.sciencedirect.com/science/article/pii/S1270963817305497

[11] S. Tian, D. Lin, J. Wang, and B. Li, "Dynamic stability of rolling missiles with angle-of-attack feedback three-loop autopilot considering parasitic effect," *Aerosp. Sci. Technol.*, vol. 71, pp. 592–602, Dec. 2017. [Online]. Available: http://www.sciencedirect.com/science/article/pii/S1270963817311550

[12] W. Li, Q. Wen, and Y. Yang, "Stability analysis of spinning missiles induced by seeker disturbance rejection rate parasitical loop," *Aerosp. Sci. Technol.*, vol. 90, pp. 194–208, Jul. 2019. [Online]. Available: http://www.sciencedirect.com/science/article/pii/S1270963818309477

[13] Q. Wen, T. Lu, Q. Xia, and Z. Sun, "Beam-pointing error compensation method of phased array radar seeker with phantom-bit technology," *Chin. J. Aeronaut.*, vol. 30, no. 3, pp. 1217–1230, 2017. [Online]. Available: http://www.sciencedirect.com/science/article/pii/S1000936117301000

[14] T. Dowling, L. Lewis, and A. Chinchillo, "Radome computer compensation," in *Proc. Antennas Propag. Soc. Int. Symp.*, vol. 17, Jun. 1979, pp. 602–605. [Online]. Available: http://ieeexplore.ieee.org/document/1148090/

[15] R. Das, "Advances in active radar seeker technology," *Defence Sci. J.*, vol. 55, no. 3, pp. 329–336, 2005.

[16] I. Klein and I. Rusnak, "Loop-shaping approach to mitigate radome effects in homing missiles," *J. Guid., Control, Dyn.*, vol. 40, no. 7, pp. 1789–1795, Jul. 2017. [Online]. Available: https://arc.aiaa.org/doi/10.2514/1.G000850

[17] R. Zong, D.-F. Lin, L. Lan, and H. Wang, "Influence of radar seeker disturbance rejection rate with radome error and on-line compensation with UKF," *Trans. Beijing Inst. Technol.*, vol. 36, pp. 1269–1278, Dec. 2016. [Online]. Available: http://www.cnki.com.cn/Article/CJFDTOTAL-BJLG201612012.htm

[18] H. Oulei, W. Jiang, L. Defu, and H. Dingding, "Online compensation method for disturbing torque of laser gimbaled seeker using STUKF," *Infr. Laser Eng.*, vol. 45, no. 12, 2016, Art. no. 1217006. [Online]. Available: http://www.opticsjournal.net/Abstract.htm?id=OJ170103000139bIeKhN

[19] W. Bai, W. Xue, Y. Huang, and H. Fang, "On extended state based Kalman filter design for a class of nonlinear time-varying uncertain systems," *Sci. China Inf. Sci.*, vol. 61, no. 4, Apr. 2018, Art. no. 042201. [Online]. Available: http://link.springer.com/10.1007/s11432-017-9242-8

[20] W. Liu, X. Wang, and Z. Deng, "Robust Kalman estimators for systems with multiplicative and uncertain-variance linearly correlated additive white noises," *Aerosp. Sci. Technol.*, vol. 72, pp. 230–247, Jan. 2018. [Online]. Available: http://www.sciencedirect.com/science/article/pii/S1270963816305983

[21] B. Gao, S. Gao, G. Hu, Y. Zhong, and C. Gu, "Maximum likelihood principle and moving horizon estimation based adaptive unscented Kalman filter," *Aerosp. Sci. Technol.*, vol. 73, pp. 184–196, Feb. 2018. [Online]. Available: http://www.sciencedirect.com/science/article/pii/S1270963817305552

[22] B. T. Burchett, "Unscented Kalman filters for range-only cooperative localization of swarms of munitions in three-dimensional flight," *Aerosp. Sci. Technol.*, vol. 85, pp. 259–269, Feb. 2019. [Online]. Available: http://www.sciencedirect.com/science/article/pii/S1270963818317796

[23] S. Lin, W. Wang, W. Lin, and C. Li, "The research of loop-shaping method to mitigate the total error effect in air-to-air missiles," *Optik*, vol. 181, pp. 923–932, Mar. 2019. [Online]. Available: http://www.sciencedirect.com/science/article/pii/S0030402618320965

[24] R. C. Dorf and R. H. Bishop, *Modern Control Systems*. London, U.K.: Pearson, 2011.

[25] B.-Z. Guo and Z.-L. Zhao, "On the convergence of an extended state observer for nonlinear systems with uncertainty," *Syst. Control Lett.*, vol. 60, no. 6, pp. 420–430, 2011. [Online]. Available: http://www.sciencedirect.com/science/article/pii/S016769111100065X

SHIH-YAO LIN received the M.S. degree from the School of Aerospace Engineering, Beijing Institute of Technology, in 2018, where he is currently pursuing the Ph.D. degree. He focuses on the flight vehicle guidance and control, and electrical design.

DEFU LIN received the Ph.D. degree from the School of Aerospace Engineering, Beijing Institute of Technology, in 2004. He is currently the Head of the Institute of UAV Autonomous Control, and also the Director of the Beijing Key Laboratory of UAV Control. He is also a Professor of flight vehicle design with the Beijing Institute of Technology. He focuses on the overall design of fixed-wing and rotor-wing flight vehicle.

WEI WANG received the Ph.D. degree from the School of Aerospace Engineering, Beijing Institute of Technology, Beijing, in 2015. He is currently a Lecturer with the School of Aerospace Engineering, Beijing Institute of Technology. His research interests include flight vehicle design, aerodynamics, guidance and control, and electrical design.